Acta Materialia 123 (2017) 82–89

Contents lists available at ScienceDirect

Acta Materialia

journal homepage: www.elsevier.com/locate/actamat

Full length article

Size dependent spinodal decomposition in Cu-Ag nanoparticles

G. Radnóczi [a, *], E. Bokányi [a], Z. Erdélyi [b], F. Misják [a]

[a] Research Centre for Energy Research, Hungarian Academy of Sciences, H-1525, Budapest, PO Box 49, Hungary
[b] Department of Solid State Physics, University of Debrecen, PO Box 2, H-4010, Debrecen, Hungary

ARTICLE INFO

Article history:
Received 30 May 2016
Received in revised form
10 October 2016
Accepted 16 October 2016
Available online 24 October 2016

Keywords:
Cu-Ag nanoparticles
Spinodal decomposition
Size dependence
Composition dependence
Calculation of critical wavelength

ABSTRACT

Nanoparticles are of considerable interest, owing to their size-dependent properties, different from those of bulk materials. For revealing internal atomic processes in them, individual nanoparticles of Cu-Ag alloys were grown by direct current (DC) magnetron sputtering. Phase-separation during growth in Cu-Ag particles was found to be size- and composition-dependent. Particles below 5 nm in diameter grow as a solid solution of the components for all compositions (15–80 at.% Ag). In the low Ag content range (15 and 30 at.% Ag) phase-separation occurs only for particles above 5 nm in diameter. The separation into Cu-rich and Ag-rich domains, when observed, takes place by spinodal decomposition for all particle sizes. In particles undergoing incomplete coalescence, phase-separation occurs even if the diameter of the colliding particles is below 5 nm. In the higher Ag content range (60–80 at.%), however, no phase-separation is observed until coalescence sets in. Lattice parameter measurements in alloy particles of 30 at.% Ag revealed that the miscibility gap in individual particles varies between 70 and 90 at.%. Calculation of the composition dependence of the critical length for spinodal decomposition provided quantitative explanation for the observed phenomena.

1. Introduction

Nanoparticles are of considerable interest, as they often possess size-dependent properties, different from those of bulk materials. In the last few years, many investigations have focused on bimetallic nanoparticles, owing to their promising characteristics. Both one-phase and two-phase alloy nanoparticles are of great interest for their improved chemical [1,2], catalytic [3], optical [4], biological [5] and plasmonic [6] properties over their single-component counterparts.

Specific physical and other properties of nanoparticles depend on their atomic structure and arrangement of the component atoms. It is likely that the structure formation of alloy phases in the nanosize region also takes place in a distinctive way, different from that in the bulk.

Alloy nanoparticles can be produced by different methods; chemical and electrochemical techniques have high efficiency. Thin (5 nm and below) noble metal deposits on substrates present a simple one-step, reproducible way to make stable nanostructures. Physical methods are adequate to grow alloy nanoparticles on a substrate, both by sequential- or co-deposition of otherwise immiscible components. Sequential deposition will essentially result in core-shell morphology, while co-deposition opens the possibility for mixing other ways immiscible components. In co-deposited alloys of components having limited solubility in each other different kinds of metastable/unstable structures can form which can spontaneously undergo phase transformation/phase-separation still during or after the growth. Nevertheless, if understood, these processes offer new possibilities for designing or controlling the structure and through that the properties of nanoparticles. A promising system for investigation of these kinds of phenomena can be composed from components having broad miscibility gap. Systems with the ability to undergo spinodal decomposition are especially promising.

A typical example of a binary system with large miscibility gap is the Cu-Ag system. Concerning the phase state of Cu-Ag nanoparticles, only minor changes in the actual phase diagram of nanoparticles was predicted, in comparison to the equilibrium one measured for the bulk Cu-Ag system [7,8]. In addition, no spinodal decomposition was observed in nanoparticles of eutectic composition of about 10 nm in size [9]. On the contrary, larger deviations from equilibrium processes were observed by H.T. Hai et al. [1]. They showed that in Ag-Cu core-shell particles, the agglomeration of Ag takes place above 150 °C. For particles below 50 nm this

* Corresponding author.
E-mail address: radnoczi@mfa.kfki.hu (G. Radnóczi).

http://dx.doi.org/10.1016/j.actamat.2016.10.036
1359-6454/

process was found to be diffusion-controlled with activation energy of 37.56 kJ/mol. This corresponds very well to the activation energy for the surface diffusion of Ag [1]. It has also been shown [10] that the spinodal curve and the miscibility gap both shrink as the particle size decreases, even in the absence of relatively larger surface effects. Larger surface effects experienced by smaller particles have been supported by calculations with a phase-field model [11]. However, it has also been shown experimentally that a thin carbon coating can reduce these surface effects, and prevent the surface-induced reduction of the miscibility gap [12]. The atomic structure and the morphology can vary from (meta)stable solid solutions to two-phase particles with core-shell or side-segregated morphology. The level of separation of the components (the width of the miscibility gap) can also depend on the size and the composition of the particles.

In the present work, phase-separation in Cu-Ag co-deposited nanoparticles has been investigated. The Cu-Ag system, a typical eutectic which has a wide miscibility gap, has been chosen for its relative chemical inertness and ability for spinodal decomposition [13,14]. Both Cu and Ag have fcc symmetry of lattice parameters 0.3615 and 0.4085 nm, respectively. The solubility at room temperature of these components in each other is negligible in equilibrium conditions. However, co-deposition at room temperature and below can lead to the formation of crystalline [15] and even amorphous [16] solid solutions. Spinodal decomposition in thicker Cu-Ag films has been found to be a working atomic mechanism of the nanocomposite structure formation, at compositions close to eutectic (60 at.% of Ag) [14]. For discontinuous yet Cu-Ag films, liquid–like coalescence resulted in random two-phase polycrystalline islands, owing to crystallization from the melt [14].

Preparation of Cu-Ag alloy nanoparticles by co-deposition, as well as their phase-separation processes, including spinodal decomposition, is studied in this work. The demand to understand morphological development and stability in these nanostructures has an increasingly growing importance, as two- and multicomponent nanoparticles are gaining application. The results are treated in the frames of the Chan-Hillard theory of spinodal decomposition.

2. Materials and methods

The nanoparticles were prepared using DC magnetron co-deposition of Ag and Cu on thin amorphous carbon film in Ar atmosphere of 0.2 Pa pressure. The deposited quantities of Cu/Ag mixtures were grown to a very small effective thickness, about 1 nm, to result in individual nanoparticles. At this point, the deposition process was stopped providing the possibility to investigate the properties of separate nanoparticles formed at the very beginning of the deposition process – before coalescence and continuous film formation.

During the process, the background vacuum was about 8×10^{-6} Pa. The two sputtered targets consisted of 99.99% pure Cu and Ag. The sputtering speed ranged between 0.1 and 1 nm/s, and was controlled by the sputtering power of the targets. All depositions were made at ambient temperature (about 20 °C) and floating potential of the substrate onto thin amorphous carbon substrates. The composition was controlled by setting the appropriate growth rates for the components after calibration. In order to confirm the resultant compositions, energy dispersive X-ray spectroscopy (EDS) analysis was carried out. The composition of the samples covered several different values between 15 at.% Ag and 80 at.% Ag.

The samples were examined by transmission electron microscopy (TEM) in a Philips CM20 electron microscope operated at 200 kV. As a result of the thin substrate, the samples were suitable for TEM analysis without further preparation. This allowed the examination of the obtained nanoparticles in a very short time after growth. Analytical measurements were carried out using a NORAN Energy Dispersive Spectrometer (EDS), with a Ge detector attached to the CM20 microscope. High-resolution TEM (HREM) measurements were performed in a JEOL 3010 microscope at 300 kV accelerating voltage close to Scherzer defocus values. A built-in Fourier-transform algorithm of the Digital Micrograph software was used for quantitative analysis of the HREM images.

3. Results

Samples grown in the whole composition range to an effective thickness of about $t = 1$ nm formed individual nanoparticles on the amorphous carbon substrate. A typical array of such particles is shown in Fig. 1 for an alloy of 60 at.% Ag content. The size of the particles is a few nm in diameter, most of them being of hemispherical shape. Faceting of a few of them could also be observed. Most particles in our experiments are the result of individual crystal growth from the vapour phase and the collection of adatoms from a substrate area (particles denoted A in Fig. 1). However, in some cases, the individual crystals are able to reach the growth stage of the very beginning of coalescence. In this case a fraction of particles will be the result of coalescence (particles denoted B in Fig. 1). The distance between the centres of particles is typically about $s = 5–10$ nm, corresponding to the size of the diffusion zones where the particles form. The volume of arriving material to such a zone is $V_z = s^2t$; $t = 1$ nm and the volume of a particle is about $V_p \approx 4r^3\pi/6$ for a half-sphere of radius r. From $V_z = V_p$ we obtain (if re-evaporation is neglected) a particle diameter 2r of about 5 nm, which corresponds fairly well to Fig. 1. The actual diameter of the particles varies between 2 and 10 nm for each composition. This can be attributed to the local differences in relative configuration of the growing islands on the substrate, as well as to occasional coalescence events. Despite these differences between individual particles within one sample we consider them having the same composition.

According to electron diffraction the 60 at.% Ag content sample consists of one-phase solid solution particles. The crystallographic

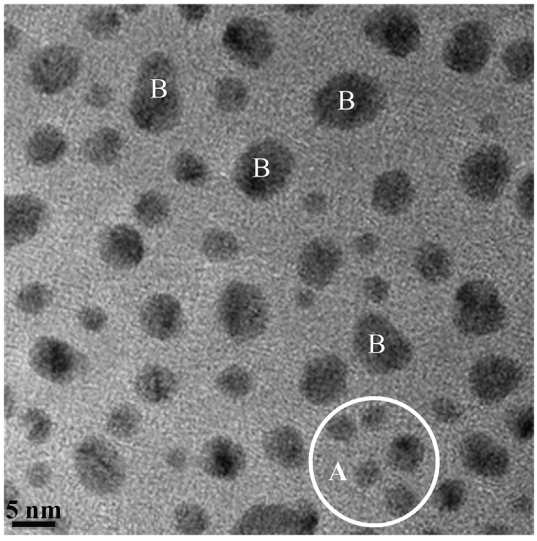

Fig. 1. Overall view of Cu-Ag alloy nanoparticles (60 at.% Ag content), formed by co-deposition (about ~1 nm effective thickness). Particles marked by A and similar are the result of individual growth; those marked by B have undergone coalescence. The light grey background corresponds to the carbon substrate.

orientation of the particles is random. This should be the case on an amorphous substrate, where texture usually develops during coalescence [17]. The random orientation of the islands also proves that they are in the growth stage preceding or at the very beginning of coalescence.

To reveal the phase state of the individual particles, high-resolution microscopy was used. High-resolution images allow the visualization of lattice fringes in the particles and the measurement of their spacing. Fast Fourier Transform (FFT) of the images shows the spectrum of the lattice distances imaged in the particles, and reveals if they have a one- or two-phase structure.

For the quantitative analysis of phase-separation in individual particles, the measurement of the lattice distances imaged in them can provide further information. Eq. (1) shows the relation between the lattice parameter of a solid-solution alloy and its pure components, where x denotes the concentration of Ag in mole fractions, and a_{Cu} and a_{Ag} denote the lattice parameter of pure copper and silver, respectively.

$$x_{alloy} = (1-x)a_{Cu} + xa_{Ag} \quad and \quad x = \left(a_{alloy} - a_{Cu}\right) \Big/ \left(a_{Ag} - a_{Cu}\right) \tag{1}$$

The deviation from this linear law discussed in Refs. [18 and 19] is hardly resolvable with the electron diffraction methods applied here, so will be neglected in further discussions.

Assuming a linear dependence between the composition and the lattice parameters (Eq. (1)), the estimation of the solute content becomes possible with the help of the measurement of lattice spacing and the determination of corresponding Miller indices.

The FFT diffraction patterns of nanoparticles taken from an area of 42 × 42 nm, similar in structure to that shown in Fig. 1, are shown in Fig. 2. The FFT diffraction pattern in Fig. 2a shows the two-phase (Ag and Cu) nature of the sample (30 at.% Ag), proving that phase-separation occurred in the nanoparticles. The peculiarity of the diffraction is the occurrence of Cu 111 and Ag 111 reflections in pairs, indicating that these pairs originate from Cu and Ag crystallites having epitaxial relation to each other. The difference in diameter between the Ag 111 and Cu 111 rings corresponds to 0.024 nm in the spacing of {111} planes of the separated phases (Ag and Cu). This is about 11% less than the difference, corresponding to complete separation (0.0272 nm). According to Eq. (1) it denotes the formation of two solid solutions with ~89 at.% concentration difference (miscibility gap) on average. However, the distance between the pairs of diffraction spots varies from reflection to reflection (Fig. 2a), indicating a difference in the level of separation of the components from particle to particle.

The FFT of the particles with composition of 80 at.% Ag (Fig. 2b) shows no epitaxial relation between reflections. According to this, we assume that the same phase-separation as seen in Fig. 2a cannot be detected in this sample. Consequently, these particles have single-phase structure and the reflections on the two rings belong to one fcc phase. The reflections falling outside the dotted circles (marking pure Ag) in Fig. 2b correspond to alloy formation, with a decreased lattice parameter compared to Ag, as expected from Eq. (1).

Besides the FFT analysis of the HREM images we investigated the structure of individual particles as well. Based on this analysis, made for different compositions, the particles could be divided into two-phase and single-phase ones. We found that the phase-state depends on the diameter and composition of the nanoparticles. Fig. 3a shows for 30 at.% Ag content that particles of about 3 nm in diameter have single-phase structure, while larger ones (just above 5 nm and about 8 nm in diameter) are two-phase particles. Moreover, in the two-phase particles the phases are epitaxial with each other as identified by the position of their 111 reflections. These particles are composed of two and three Cu and Ag rich domains, accordingly. For 60 at.% Ag content most particles prove to be single-phase solid solutions, independent of their size, as shown in Fig. 3b.

The results of measurements for all investigated compositions (15, 30, 60, 70 and 80 at.% Ag) conclude that particles of all compositions of size below about 5 nm show a single-phase structure of a solid solution. Above this size, the phase state of a particle (formation of single- or two-phase structure) depends on composition. For compositions 15 and 30 at.% of Ag particles which were larger than 5 nm tend to have a two-phase structure, while for samples of Ag content above 60 at.% mainly single-phase particles are typical.

According to [20] and [21], the occurrence of phase-separation is size-dependent in alloy particles. 7 nm is given as the lowest size limit of phase-separation for Ag-Ni alloy particles in Ref. [21]. In the present work, for co-sputtered Cu-Ag particles 5 nm is observed as the characteristic size of the formation of two-phase particles. Nevertheless, Fig. 3 shows an increase in the characteristic size with increasing Ag content. Actually no phase-separation was observed for particle sizes up to 10 nm in alloys of 60 at.% Ag content and above. According to [9], nanoparticles of eutectic Cu-Ag alloy (60 at.% Ag) prepared by solvothermal synthesis revealed no phase-separation up to 230 °C. This is in accordance with the present

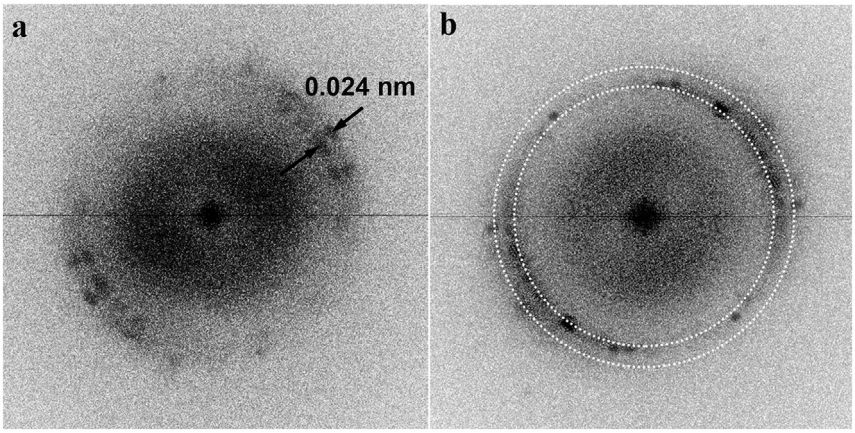

Fig. 2. Fast Fourier Transform of a HREM image of nanoparticles of (a) 30 at.% of Ag and (b) 80 at.% Ag content. The image in a) reveals the two-phase structure of the particles and the difference in diameter between the Ag 111 and Cu 111 rings corresponds to 0.024 nm in the spacing of {111} planes of the separated phases. The image in b) shows diffraction from a single phase fcc structure, the dotted lines show the position of the Ag 111 and 200 rings.

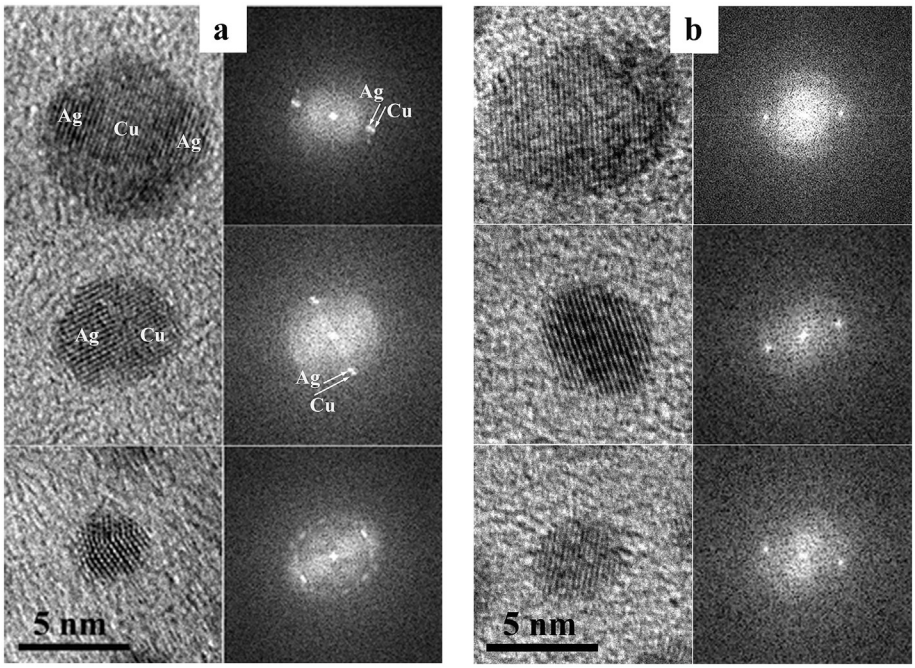

Fig. 3. HREM images of Cu-Ag nanoparticles in (a) 30 at.% Ag and (b) 60 at.% Ag particles and the corresponding FFT diffractions. From both concentrations and size a typical particle was chosen as a representation. Phase-separation is observed in particles larger than 5 nm and for Ag content of 30 at.% (diffraction dots are doubled in the FFT diffraction; similarly as in Fig. 2a). Only one-phase particles are found for above 60 at.% Ag content. The denoted Ag and Cu domains within two particles are identified according to their lattice parameters (for Ag domains ~0.235 nm and for Cu ones ~0.208 nm; the transition from Ag to Cu structure is gradual, no sharp interface between them) and can be recognized by change of fringe spacing in the pictures.

observations, though the average particle diameter in Ref. [9] was around 10 nm, somewhat bigger than in the present measurements (Fig. 1). For Cu-Ag alloy particles of larger sizes Chen, H. and J.-M. Zuo [20] observed enhanced phase-separation with increasing particle size (from 2.8 to 8.4 nm effective film thickness) for 50 at.% Ag films and mostly in coalescing particles.

These facts allow the conclusion that particle size and composition play important role in the phase-separation mechanism of Cu-Ag alloy particles: particles with 15 and 30 at.% Ag content start separation above 5 nm diameter; in particles of Ag content above 60 at.% Ag this process takes place only above 10 nm diameter.

Many of the single-phase particles are defect-free single crystals (Fig. 3). A typical example is additionally shown in (Fig. 4a), where a particle (60 at.% Ag) of [001] orientation is selected. A part of particles in the size region below 5 nm is, however, defective; the typical defect being twinning in them independent on composition. Fig. 4b and c shows particles, composed of coherent twins, all parts of which share a common <110> type direction parallel to the substrate normal. An example of regular multiple twinning is demonstrated by the particle shown in Fig. 4c. Here the twin formation is repeated on alternate {111} twin planes so as to form circular arranged twins of (close to) fivefold symmetry, sharing also a common <110> axis. Fivefold twinning has been discussed and observed in many other fcc metal and alloy nanoparticles [22,23]. The Cu-Ag alloy is another example of their formation.

The diffraction pattern of the particle in Fig. 4c also indicates a one-phase alloy with a = 0.403 ± 0.004 nm as lattice parameter, which is about 1.3% smaller than the bulk value for Ag. According to eq. (1), this corresponds to 11 at.% Cu content against the nominal 20 at.% of Cu. Segregation of Cu, tensile strain owing to the fivefold structure and formation of some Cu-oxide, can be responsible for the apparently missing Cu content, as estimated from the lattice parameter change. Many of the examined single phase particles (⌀ = 5–10 nm in the range of 60–80 at.% of Ag) are also defective: not only is twinning present, but also stacking faults are appearing. The defective nature of the particles does not seem to affect the stability of these particles against decomposition.

3.1. Phase-separation in Cu-Ag particles of 30 at.% Ag content

In the larger particles (⌀ = 5–10 nm) containing less than, or equal to 30 at.% of Ag, the occurrence of phase-separation becomes significant. Fig. 5 shows the statistics of the measured lattice distances in a sample of 30 at.% Ag, with no respect to particle size. The absolute values measured from the micrographs can depend on the magnification calibration of the images, however, the relative values can be considered to be correct.

If there was only a homogeneous alloy of the nominal composition (30 at.% Ag), there would only be one 111 spacing located between the values of 111 spacing of the pure Ag and Cu (eq. (1)). However, in our case, there are two larger maxima and even a third small maximum between them. The two larger peaks are close to 111 spacing of Ag and Cu but they are located closer than they would be for pure components. This indicates that the separation has not finished with the formation of pure Cu and Ag but Cu-rich and Ag-rich solid solution phases have formed. The estimation (eq. (1)) of the concentration difference between the Cu-rich and Ag-rich phases is about 85 at.%, on average, which can be considered as the average miscibility gap in them. The third small maximum corresponds to 111 spacing of a Cu-Ag alloy (Fig. 5). This can be explained by the presence of small (⌀<5 nm) particles that form a homogeneous solid solution. This fits well with the result of the above discussion and with Fig. 3.

There are also a few values exceeding the lattice parameter value of pure Ag. This must be a result of different size effects [24,25] or measurement errors. An individual example is shown in Fig. 4a. For this particle, the lattice spacing of the {200} type planes is measured to be 0.207 ± 0.003 nm, though it should be below

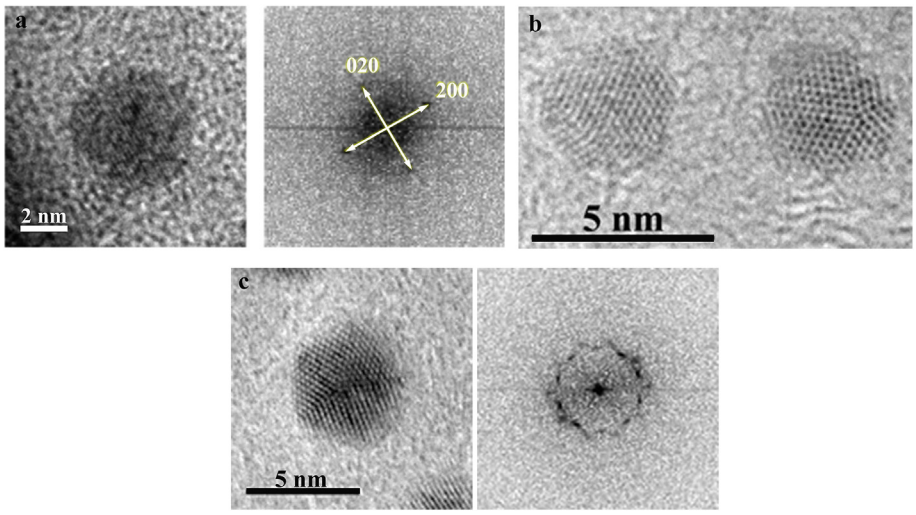

Fig. 4. High resolution images of (a) single-phase, defect-free 60 at.% Ag alloy particle of [001] orientation; (b) 80 at.% of Ag alloy single-phase twinned nanoparticles; and (c) a pentagonal multiple-twinned nanoparticle. Faceting of the particles is evident in (b) and (c).

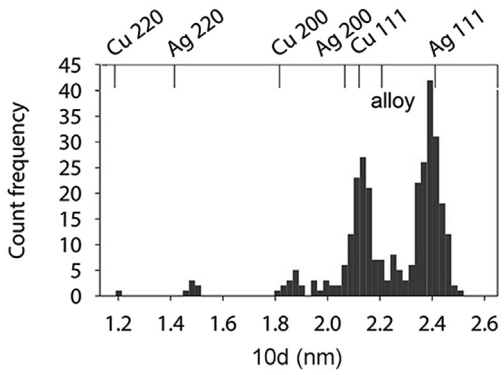

Fig. 5. Distribution of measured lattice distances in the 30 at.% Ag sample. Pure Cu and Ag parameters (obtained from X-ray diffraction database) are indicated by markers. The 111 spacing for the expected homogeneous alloy of this composition (Eq. (1)) is also indicated.

0.204 nm (it should be 0.199 nm in the case of 60 at.% Ag alloy).

For two-phase particles of the 30 at.% Ag sample (see e.g. examples in Fig. 2a) the distribution of differences between the 111 spacing of Ag-rich and Cu-rich domains $\Delta d(111) = d_{111}(Ag)\text{-}d_{111}(Cu)$ across the phase boundary in individual particles was also determined (Fig. 6). In the case of complete separation the difference of 111 lattice spacing of pure components should correspond to 0.027 nm. The most frequent difference is 0.024 nm. The concentration gap calculated from this distance equals to ~89%, which agrees well with the result obtained from Fig. 5. There remains, however, a number of boundaries across which the $\Delta d(111)$ difference is smaller and accordingly the separation is less complete. For example, at $\Delta d(111) = 0.020$ nm the concentration difference on the two sides of a phase boundary corresponds to 74 at.%. The $\Delta d(111)$ differences larger than for pure components must be a result of measurement errors or different size or shape- [24,25], as well as other effects causing changes in the lattice spacing.

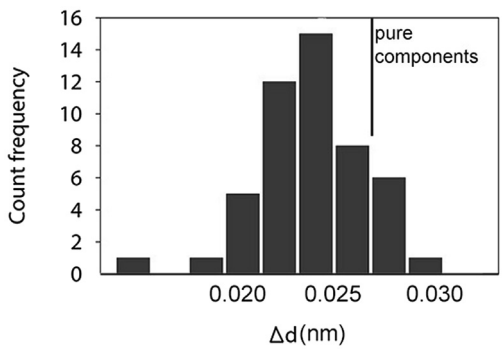

Fig. 6. Distribution of $d_{111}(Ag)\text{-}d_{111}(Cu)$ calculated from 111 epitaxial reflections in phase-separating particles of 30 at.% Ag content sample. Frequency of occurrence is shown as the function of the difference.

Despite the fact that the accuracy of the measured lattice spacing differences has certain limitations, the obtained width of the average miscibility gap from three different measurements (Figs. 2, 5 and 6) is practically the same (85–89 at.%). This can be considered a relatively safe estimation of the width of the miscibility gap in individually grown Cu-Ag nanoparticles of 30 at.% Ag content, and particle diameter of 5–10 nm.

3.2. Phase-separation in coalescing Cu-Ag particles

At the growth conditions used in our experiments two types of coalescence can occur in the case of nm-size particles [17]. The coalescence is complete when a single crystal particle forms from two (or more) particles. The process can take place in liquid or solid state. Liquid state coalescence results in the melting of coalescing particles, then the new crystal forms by the solidification of the melt. Solid-state coalescence occurs by diffusion processes. The result of complete coalescence cannot be distinguished from the crystallites grown individually from the vapour phase. Incomplete coalescence occurs when a grain or phase boundary between the coalescing particles is incorporated in the resulting one. Particles having undergone incomplete coalescence are analysed in Fig. 7.

Two coalescing particles of sample (30 at.% of Ag), are presented in Fig. 7a. Two distinct lattice plane distances are displayed in each of them. The FFT pattern (Fig. 7d or e.) also shows the corresponding two distances with two pairs of 111 reflections positioned epitaxially to each other. Shorter 111 reciprocal vectors correspond to the larger lattice spacing of an Ag-rich alloy; longer ones correspond to a Cu-rich alloy. Filtering these 111 reflection pairs, respectively, gives the location of the Ag- and Cu-rich domains after

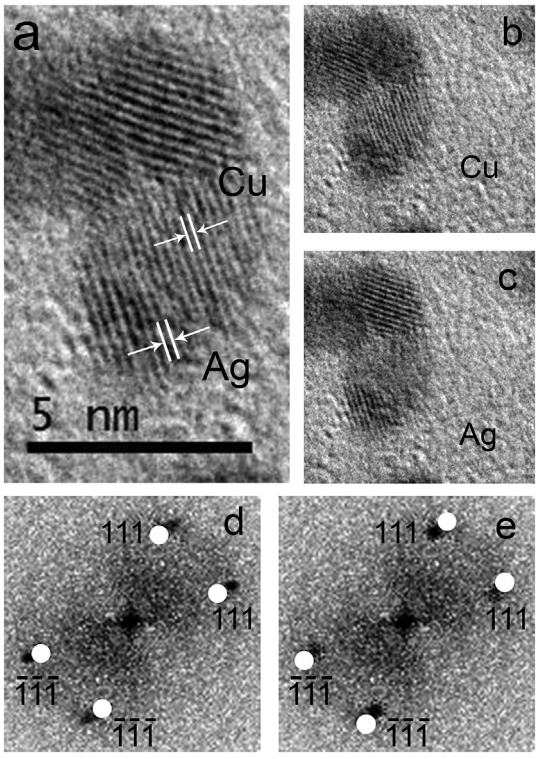

Fig. 7. HREM image of two (30 at.% of Ag) coalescing nanoparticles (a). Fourier transform with epitaxial reflections and overlaying filtering masks are shown in (d and e). Inverse Fourier transforms after filtering (a), showing Cu-rich (b) and Ag-rich (c) regions.

an inverse Fourier transformation (Fig. 7b and c.). The Cu- and Ag-rich domains are placed adjacent to each other in the particles, with a coherent phase boundary present. Their lattice fringes, visible in Fig. 7a, extend through the phase boundary continuously showing epitaxial relation. From the measured parameters the phase-separation corresponds to ~70 and ~80 at.% concentration difference in the two particles (Eq. (1)). As the fringes are inclined to the phase boundary, misfit dislocations should be seen, but are not detected in it. The full misfit between pure Cu and Ag is close to 12% (11.948%), which means that at every 9th lattice plane a misfit dislocation should be located in the phase boundary. Internal strains and decreased misfit owing to incomplete separation may have contributed to the increase of the period of misfit dislocations. The size of the particles and the length of the phase boundary are too small for a misfit dislocation to appear in Fig. 7.

The size of coalescing grains in Fig. 7 is smaller than 5 nm. Despite the fact that no phase-separation was observed in individual, single crystalline particles of this size, it is present in the coalescing (polycrystalline) ones. Obviously, the size of the coalescing island as a whole determines the critical size, where phase-separation starts. 4.

4. Evaluation and discussion of the results

The decomposition of Cu-Ag alloy films or nanoparticles is discussed in numerous works in terms of spinodal decomposition [14,21,26]. Indeed, the metastable phase diagram contains the chemical and coherent spinodals [13]. Accordingly, the decomposition of an otherwise metastable solid solution can take place either by equilibrium phase separation process through nucleation or by spinodal process. However, as long as nucleation needs large concentration fluctuations and activation to reach a critical size, the spinodal process can proceed in infinitesimal steps spontaneously.

The spinodal character of the observed decomposition in our Cu-Ag nanoparticles is supported by certain structural and morphological characteristics. On one hand epitaxial relation of the Cu-rich and Ag rich domains was observed (Figs. 2a, 3 and 7), which is an important criterion of their formation by spinodal decomposition, observed already for Cu-Ag thin films [14]. On the other hand, variation in the lattice spacing difference in individual particles (Fig. 6) shows that the separation process reaches different levels in them, proving that changes in composition occur gradually. This is, also suggesting the spinodal way of decomposition. Another indication is the similarity in the size of Cu-, and Ag-rich domains (Figs. 3a and 7), suggesting that the separation of components takes place by the formation of compositional waves. The observation of a critical particle size for starting the decomposition equals to 5 nm, which enables hosting the critical wavelength for spontaneously growing compositional fluctuations required for spinodal decomposition. Consequently, it can be proposed, that the main mechanism of phase-separation in these particles is spinodal decomposition. This argumentation, however, leaves open the question on composition dependence of the critical size for starting decomposition in particles.

Kinetic Monte Carlo and kinetic mean field simulations carried out in Refs. [27–29] for calculating compositional waves in a spinodally decomposing slab of Cu-Ag alloy resulted in 5–6 nm wavelength and practically perfect separation of the components. In nano-particles of 30 at.% Ag (Fig. 3a) the wavelength of compositional waves (the size of Cu and Ag rich epitaxial domains) is estimated to be around 5 nm suggesting that particles, hosting at least one wavelength of compositional waves reach the instability criterion and undergo spinodal decomposition. On the contrary, in Ag-rich particles, at particle sizes up to 10 nm this instability criterion is not fulfilled, the solid solution structure remains (meta) stable (Fig. 3b).

The composition dependence of the critical size can be attributed both to energetic and kinetic factors. The driving force for separation has its maximum at the composition corresponding to 40 at.% of Ag, where the free energy (Fig. 8a), the chemical and coherent spinodal curves [13] also have their maximum. This suggests faster decomposition in the Cu-rich region. An additional effect can be imposed by the dependence of the surface energy on composition [30]. The dependence of diffusion coefficients on composition [31], as well as the relation of surface and bulk diffusion coefficients, can contribute to the kinetic factors influencing phase separation. The kinetic factors can be estimated by the temperature of the growing sample. A rough estimation of the increase of the sample temperature due to impact by bombardment and heat of condensation gives $\Delta T = 20–50\ ^{\circ}C$. The sample is supported by a Cu grid hold on a massive sample holder; consequently the above numbers must be an upper limit of the temperature increase of the sample during growth and should not affect the growth kinetics substantially.

The composition dependence of the critical size can also be attributed to the composition dependence of the critical wavelength of spontaneously growing compositional oscillations. Consequently, we can suppose that the critical wavelength of unstable (growing) compositional oscillations is larger in Ag rich alloy particles than in Cu rich ones.

This argument also follows from the analysis of the electron diffraction measurements made on Cu-Ag films of different composition (Fig. 6 in Ref. [20]). There, the decomposing Cu-rich samples show much broader 111 reflections than the Ag-rich ones. This indicates a smaller size of coherently scattering domains and consequently a smaller wavelength for concentration

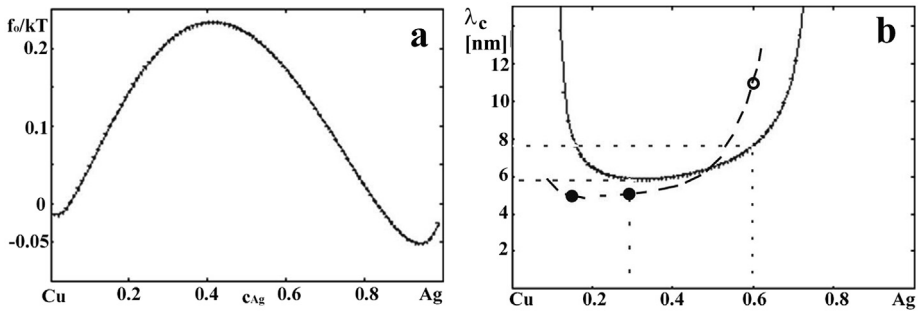

Fig. 8. Homogeneous part of the Gibbs free f_o energy (a) and critical wavelength λ_c in spinodal decomposition (b) versus composition in Cu-Ag system by eqs. (6) and (8). ($T = 873$ K, $T_c = 1053$ K, $a = 0.4$ nm). In (b) full dots mark experimental critical size, the open circle marks the estimated lower value of the critical size.

oscillations in Cu-rich samples compared to Ag-rich ones.

To estimate how the critical wavelength (λ_c) in spinodal decomposition depends on the composition, we have to solve the Cahn-Hilliard equation [32].

$$\frac{\partial \rho_A}{\partial t} = \tilde{D}\frac{\partial^2 \rho_A}{\partial x^2} - \frac{2\tilde{D}}{f''_0}\kappa\frac{\partial^4 \rho_A}{\partial x^4} \tag{2}$$

where ρ_A is the volume density of atoms A, t is the time, $\tilde{D}$ is the interdiffusion coefficient, x is the spatial coordinate, f''_0 is the second derivative by composition of the Helmholz free energy of a unit volume of homogeneous material and κ is the gradient energy coefficient. The particular solution of Eq. (2) is $\rho_A(t)$-$\rho_o = A(t)\sin(hx)$ where $h = 2\pi/\lambda$ and A is the amplitude of concentration fluctuations with a wavelength of λ. ρ_0 is the average composition. Substituting this solution into Eq. (2), we arrive to the following expression:

$$R \equiv \frac{d}{dt}\ln A(t) = -\tilde{D}\left(1 + \frac{2\kappa h^2}{f''_0}\right)h^2 \tag{3}$$

R is usually called as the amplification factor, the sign of which shows if the amplitude $A(t)$ of a concentration fluctuation with a given wavelength (λ) increases ($R > 0$) or decreases ($R < 0$) in time. The critical wavelength λ_c is, therefore, determined by the $R = 0$ condition:

$$\lambda_c = \sqrt{-\frac{8\kappa\pi^2}{f''_0}} \tag{4}$$

When the system is phase-separated into high and low composition regions $\kappa = \xi^2 kT$[10], where k and T are Boltzmann's constant and the absolute temperature, respectively, and ξ is the length, scaling with the width of the interface. Furthermore, $\xi \approx 2d(T_c/T_c\text{-}T)^{1/2}$[33], where d is the interatomic distance and T_c is the maximum temperature of the miscibility gap ($T_c = 1053$ K). In a fcc lattice $d^2 = a^2/2$, where a is the lattice parameter, therefore

$$\kappa \approx a^2\frac{2T_c}{T_c - T}kT \tag{5}$$

The Gibbs free energy density in the solid and homogeneous Ag-Cu system can be described by the following polynomial [34]

$$f_0 = f_{0Ag}c + f_{0Cu}(1-c) + kT[c\ln c + (1-c)\ln(1-c)] + Vc(1-c) + V'c(1-c)(2c-1), \tag{6}$$

where $f_{0Ag} = -11945 + 9.67T$, $f_{0Cu} = -13054 + 9.62T$, $V = 34532 - 9.178T$, $V' = -5996 + 1.725T$ (in J/mol and J/molK units) and c is the atomic fraction of Ag. By deriving Eq. (6) by c

$$f''_0 = \frac{kT}{c(1-c)} - 2V + 6V'(1-2c). \tag{7}$$

Substituting Eqs. (5) and (7) into Eq. (4), we get

$$\lambda_c = \sqrt{\frac{8}{2\frac{V}{kT} - 6\frac{V'}{kT}(1-2c) - \frac{1}{c(1-c)}}}\sqrt{\frac{2T_c}{T_c - T}}\pi a \tag{8}$$

As an illustration, Fig. 8a shows f_o the Helmholtz free energy in kT units, and Fig. 8b shows λ_c as a function of composition. As can be seen, the width of the miscibility gap is about 93% and the minimum of λ_c is at about 6 nm at 30 at.% of Ag. With increasing Ag content, however, λ_c increases more and more rapidly; tends to infinity when approaching the spinodal composition (f''_0=0). In Fig. 8b the measured critical sizes are also shown for 15 and 30 at.% Ag content particles (full dots). At 60 at.% Ag content we marked the lower estimated value of the critical size (open circle). The experimental points suggest that the real λ_c(c) curve, valid for nanoparticles, can be shifted to lower concentrations compared to the calculated curve, accepting that the critical size = λ_c(c). The reason can be the size dependence of the free energy and/or segregation of one of the components, affecting the free energy but also the composition of particles in which the spinodal process is taking place. Moreover, the calculated curve corresponds to $T_c = 1053$ K and T = 873 K, substantially higher than the deposition temperature (300 K). These temperatures, however, can be validated by the high energy of the impinging species from the plasma during growth, heat of condensation of atomic species and small size of the particles. They were used to match the λ_c(c) curve close to experimental values and in some sense give an estimation of the effective temperature of the particles what means about 500 K effective temperature increase (in other words about 500 K decrease of their melting temperature) [35].

5. Conclusions

Phase separation has been studied during growth of DC magnetron sputtered Cu-Ag alloy nanoparticles. The spontaneous formation of two phase nanoparticles depends on particle size and composition.

Particles below 5 nm diameter grow as a solid solution of the components for all measured compositions (15–80 at.% Ag). Phase-separation occurs above 5 nm particle diameters in the 15 and 30 at.% Ag composition range. The separation into Cu-rich and Ag-rich domains was revealed to take place by spinodal decomposition. Lattice parameter measurements in alloy particles of 30 at.% Ag revealed that the miscibility gap in individual particles varies

between 70 and 90 at.% the average being 85–89 at.%. Phase-separation in particles undergoing incomplete coalescence occurs even when the size of coalescing grains is below 5 nm.

In higher Ag content films (60–80 at.%) no phase-separation is observed until coalescence sets in (about 10 nm of particle size).

The critical size of particles above which phase-separation takes place is suggested to be connected to the composition-dependent critical wavelength of fast-growing concentration fluctuations (instability of the solid solution state). Calculation of the critical wavelength and its composition dependence result in quantitative estimation for the composition dependence of the critical size for starting spinodal decomposition in Cu-Ag nanoparticles. It gives 6 nm for the critical size for 30 at.% Ag content particles and a size of 8 nm for 60 at.% of Ag. These sizes correspond fairly well to the experimental results of 5 nm and >10 nm, respectively.

Acknowledgments

The authors acknowledge the financial support of the Hungarian Academy of Sciences under the grant OTKA-K81808, NN OTKA 112156 and NF 101329 and GINOP-2.3.2-15-2016-00041.

F. Misják also acknowledges the support of the János Bolyai Research Scholarship of the Hungarian Academy of Sciences.

References

[1] H.T. Hai, H. Takamura, J. Koike, Oxidation behavior of Cu–Ag core–shell particles for solar cell applications, J. Alloys Compd. 564 (2013) 71–77.
[2] Chi-Hang Tsai, Shin-Jun Chen, Jen-Ming Song, In-Gann Chen, Hsin-Yin Lee, Thermal stability of Cu@Ag core–shell nanoparticles, Corros. Sci. 74 (2013) 123–129.
[3] A. Sárkány, O. Geszti, G. Sáfrán, Preparation of Pdshell–Aucore/SiO2 catalyst and catalytic activity for acetylene hydrogenation, Appl. Catal. A General 350 (2) (2008) 157–163.
[4] José Luis Jiménez Pérez, Rubén Gutiérrez-Fuentes, José Francisco Sánchez Ramírez, Omar Uriel García Vidal, Daniel Erick Téllez-Sánchez1, Zormy Nacary Correa Pacheco1, Alfredo Cruz Orea, Jesús Antonio Fuentes García1, Nonlinear coefficient determination of Au/Pd bimetallic nanoparticles using Z-scan, Adv. Nanoparticles 2 (2013) 223–228.
[5] Kuan-ting Chen, Dahtong Ray, Yu-hsien Peng, Yu-Chi Shu, Preparation of CueAg coreeshell particles with their anti-oxidation and antibacterial properties, Curr. Appl. Phys. 13 (2013) 1496–1501.
[6] Prathamesh Pavaskar, I-Kai Hsu, Jesse Theiss, Wei Hsuan Hung, Stephen B. Cronin, A microscopic study of strongly plasmonic Au and Ag island thin films, JAP 113 (2013) 034302.
[7] T. Tanaka, S. Hara, Thermodynamic evaluation of nano-particle binary alloy phase diagrams, Z. Met. 92 (2001) 1236–1241, 11.
[8] S. Bajaj, M.G. Haverty, R. Arróyave, W.A. Goddard III, S. Shankar, Phase stability in nanoscale material systems: extension from bulk phase diagrams, Nanoscale 7 (2015) 9868–9877.
[9] J. Sopoušek, J. Pinkas, P. Brod, J. Buršík, V. Vykoukal, D. Škoda, A. Stýskalík, O. Zobai, J. Vlešál, A. Hrdlilka, J. Šimbera, Ag-Cu colloid synthesis: bimetallic nanoparticle characterisation and thermal treatment, J. Nanomater. 2014 (2014) 13, http://dx.doi.org/10.1155/2014/638964. Article ID 638964.
[10] D. Burch, M.Z. Bazant, Size-dependent spinodal and miscibility gaps for intercalation in nanoparticles, Nanoletters 39 (Nr. 11) (2009) 3795–3800.
[11] Ming Tang, Hsiao-Ying Huang, Nonglak Meethong, Yu-Hua Kao, W. Craig Carter, Yet-Ming Chiang, Modeling particle size effects on phase stability and transition pathways in nanosized olivine cathode particles, in: MRS Symposium Proceedings, vol. 1100, 2008, http://dx.doi.org/10.1557/PROC-1100-JJ03-04, 1100-JJ03-04.
[12] K. Zaghib, A. Mauger, F. Gendron, C.M. Julien, Surface effects on the physical and electrochemical properties of thin LiFePO4 particles, Chem. Mater. 20 (2008) 462–469.
[13] O.P. Pandey, S.N. Ojha, S. Lele, On spinodal Boundaries of the Ag-Cu system, Scripta Metallurgica Materialia 29 (1993) 1131–1134.
[14] F. Misják, P.B. Barna, G. Radnóczi, Growth of nanocomposite in eutectic Cu–Ag films, Thin Solid Films 516 (2010) 3931–3934.
[15] I. Reda, J. Hafner, P. Pongratz, A. Wagendristel, H. Bangert, B.K. Bhat, Amorphous Cu-Ag films with high stability, Phys. Status Solidi A, Appl. Res. 72 (1982) 313–324.
[16] H.W. Sheng, G. Wilde, E. Ma, The competing crystalline and amorphous solid solutions in the Ag–Cu system, Acta Mater. 50 (2002) 475–488.
[17] G. Radnóczi, P.B. Barna, in: Y. Pauleau (Ed.), Formation and Characterisation of the Structure of Thin Films and Coatings; in Materials Surface Processing by Directed Energy Techniques, Elsevier-EMRS, Amsterdam, Oxford, 2006, pp. 443–474. Ch.13.
[18] P. Duwez, R.H. Wilkens, W.J. Clement, Continuous series of metastable solid solutions in silver-copper alloys, JAP 31 (6) (1960) 1136–1137.
[19] V.A. Lubarda, On the effective lattice parameter of binary alloys, Mech. Mater. 35 (2003) 53–68.
[20] H. Chen, J.-M. Zuo, Structure and phase separation of Ag–Cu alloy thin films, Acta Mater. 55 (5) (2007) 1617–1628.
[21] C. Srivastava, S. Chithra, K.D. Malviya, S.K. Sinha, K. Chattopadhyay, Size dependent microstructure for Ag–Ni nanoparticles, Acta Mater. 59 (16) (2011) 6501–6509.
[22] H. Hofmeister, Forty years study of fivefold twinned structures in small particles and thin films, Cryst. Res. Technol. 33 (1) (1998) 3–25.
[23] H. Hofmeister, Fivefold twinning in nanosized particles and nanocrystalline thin films-ubiquitous metastable structures, J. Metastable Nanocrystalline Mater. 2–6 (1999) 325–332.
[24] W.H. Qi, M.P. Wang, Size and shape dependent lattice parameters of metallic nanoparticles, J. Nanoparticle Res. 7((2005) 51–57.
[25] C. Solliard, M. Fluelli, Surface stress and size effect on the lattice parameter in small particles of gold and platinum, Surf. Sci. 156 (1985) 487–494.
[26] K. Labisz, Z. Rdzawski, M. Pawlyta, Microstructure evaluation of long-term aged binary Ag-Cu alloy, Archives Mater. Sci. Eng. 49 (1) (2011) 15–24.
[27] Z. Erdélyi, Z. Balogh, D.L. Beke, Kinetic critical radius in nucleation and growth processes – trapping effect, Acta Mater. 58 (2010) 5639–5645.
[28] D.L. Beke, Cs Cserháti, Z. Erdélyi, I.A. Szabó, Segregation in nanostructures chapter 7, in: H.S. NALWA (Ed.), Nanoclusters and Nanocrystals, American Scientific Publishers, North Lewis Way, Stevenson Ranch, California 91381-1439 USA, 2003, p. 25650.
[29] Z. Erdélyi, D.L. Beke, Importance of proper choice of transition rates in kinetic simulations of dynamic processes, Phys. Rev. B 70 (2004) 245428.
[30] Z. Suo, W. Lu, Composition modulation and nanophase separation in a binary epilayer, J. Mech. Phys. Solids 48 (2000) 211–232.
[31] D.B. Butrymowicz, J.R. Manning, M.E. Read, Diffusion in copper and copper alloys, Part II, copper silver and copper gold systems, J. Phys. Chem. Ref. Data, 3 (Nr. 2) (1974) 527–602.
[32] A.L. Greer, F. Spaepen, Diffusion, in: L.L. Chang, B.C. Giessen (Eds.), Materials Science Series, Synthetic Modulated Structures, Academic Press Inc, 1985, pp. 419–487.
[33] J.W. Cahn, J.E. Hilliard, Free energy of a nonuniform system. I. Interfacial free energy, J. Chem. Phys. 28 (1958) 258–267.
[34] J.L. Murray, Calculations of stable and metastable equilibrium diagrams of the Ag-Cu and Cd-Zn systems, Metall. Trans. A 15A (1984) 261–268. http://link.springer.com/article/10.1007%2FBF02645110.
[35] F. Ercolessi, W. Andreoni, E. Tosatti, Melting of small gold particles: mechanism and size effects, PRL 66 (Nr. 7) (1991) 911–914.